

Density profiles of two-component Bose-Einstein condensates interacting with a Laguerre-Gaussian Beam

Anal Bhowmik¹, Pradip Kumar Mondal², Sonjoy Majumder¹,
and Bimalendu Deb³

¹Department of Physics, Indian Institute of Technology Kharagpur,
Kharagpur-721302, India.

²Department of Physics, Egra Sarada Shashi Bhusan College, Egra-721429, India.

³Department of Materials Science, Indian Association for the Cultivation of Science,
Jadavpur, Kolkata 700032, India.

E-mail: analbhowmik@phy.iitkgp.ernet.in

Abstract. The density profiles of trapped two-component Bose-Einstein condensates (BEC) and its microscopic interaction with Laguerre Gaussian (LG) beam are studied. We consider the ^{87}Rb BEC in two hyperfine spin components. The wavelength of the LG beam is assumed to be comparable to the atomic de-Broglie wavelength. Competitions between intra- and inter-component interactions produce interesting density structures of the ground state of BEC. We demonstrate vortex-antivortex interference and its dependence on the inter-component interactions and Raman transitions.

1. INTRODUCTION

Binary mixtures of Bose-Einstein condensates (BEC) of different atomic species have been the subject of intensive theoretical and experimental research [1, 2, 3, 4, 5, 6, 7, 8, 9, 10, 11, 12, 13, 14, 15, 16, 17]. The mixtures can be composed of two different alkali-metal atomic gases [18, 19, 20, 21, 22, 23, 24, 25, 26] or two different isotopes of same element [27, 28, 29, 30] or same element with different hyperfine states [1, 2, 3, 4, 31, 32] etc. These mixtures provide a unique opportunity for exploring fascinating many-body quantum physics that can not be studied with a single-component Bose-Einstein condensate. For instance, phase separation [20, 21, 22, 27], pattern formation [33, 34, 35, 36], symmetry breaking transitions [37], skyrmions [38], collective modes [4, 39], nonlinear dynamical excitations [40, 41], quantum turbulence [42] and vortex bright solitons [43] have been studied with the binary BEC. Further, a separated or resolved phase of a two-component BEC is essential for Kelvin-Helmholtz [44] and Rayleigh-Taylor instability [45].

Over the years, there have been many studies of the density structure of two-component BEC, but in all the cases, analyses were limited close to the center of the trap

[20, 21, 22]. In contrast, the density structures of two-component BEC are important when the BEC interacts with an LG beam far away from the trap center. In other words, the interaction with the LG beam may provide a means to study the matter density distributions away from the trap axis. This interaction generates quantized vortices in BEC either through Raman processes [48, 49, 50, 51] or slow light consideration [52]. Because of the meandered structure of the components, our calculations show the criss-cross behavior of two-photon Rabi frequencies for Raman transitions with increasing inter-species coupling. This behaviour provides contrast in phase density in the final state after the Raman transitions, when two-counter propagating LG beams with proper frequencies interact simultaneously at individual components. This can be observed in the interference of the vortices generated in the interaction with varying coupling strengths. Moreover, for larger values of the orbital angular momentum (OAM) of light, the interaction will largely depend on the peripheral density profile of the components.

The density phase contrast can be realized by generating a vortex-antivortex superposition of BEC. The combination of vortex-antivortex matter-wave states, generated by the superposition of vortices of opposite circulation, exhibits interesting petal-like interference structures [51, 53] and intriguing dynamics [54]. The properties of vortex-antivortex structure in binary BEC yield rich physics [55, 56, 57, 58]. Kapale *et al.* [56] proposed a scheme to create a coherent superposition of vortex-antivortex in multi-component BECs using the optical vortex. They varied the population of vortex and antivortex states by changing the two-photon detuning parameter. The superposition resembles the counter-rotating persistent currents in superconducting circuits [59, 60, 61] which are promising candidates for qubits in quantum-information processing and quantum communication networks [62].

In this paper, we develop a theory for the interaction of Laguerre Gaussian (LG) beam with binary mixtures of the BEC and investigate the variation in the superposition of vortex-antivortex structure using two-photon Raman technique. To obtain the interference pattern of vortex-antivortex states, we have calculated the Rabi frequency of two-photon stimulated Raman transitions. Interesting physics can be investigated here by analyzing the mixtures of components of BECs and their inter-component interaction strength. For example, the population of vortex states in BEC components can be tuned by changing the inter-component interaction strength.

This paper is organized as follows. In Sec. II, we discuss the theory behind the generation of vortex state in binary mixtures of BEC. In Sec. III, we study the density profiles of the ground state in detail. Also, the variation of Rabi frequency with inter-component interaction, number of particles, and the intensity of trapping potential are presented in the same section. In Sec IV, we show the change in the superposition of vortex-antivortex state for the two-component BEC of equal and unequal number of topological charges. The conclusion is outlined in Sec. V.

2. THEORY

A dilute mixture of two components of a BEC trapped in a harmonic potential is considered here. To describe the stationary ground-state of this system at zero temperature limit, one can use the coupled Gross-Pitaevskii (GP) equations [7, 8, 63, 64] in cylindrical coordinate (see APPENDIX),

$$\left[-\frac{\hbar^2 \nabla^2}{2m_1} + \frac{1}{2}m_1(\omega_\perp^2 R^2 + \omega_Z^2 Z^2) + \frac{\kappa^2}{R^2} + U_{11}|\Psi_1(\mathbf{R})|^2 + U_{12}|\Psi_2(\mathbf{R})|^2 \right] \Psi_1(\mathbf{R}) = \mu_1 \Psi_1(\mathbf{R}), \quad (1)$$

$$\left[-\frac{\hbar^2 \nabla^2}{2m_2} + \frac{1}{2}m_2(\omega_\perp^2 R^2 + \omega_Z^2 Z^2) + \frac{\kappa^2}{R^2} + U_{22}|\Psi_2(\mathbf{R})|^2 + U_{21}|\Psi_1(\mathbf{R})|^2 \right] \Psi_2(\mathbf{R}) = \mu_2 \Psi_2(\mathbf{R}) \quad (2)$$

with the normalization condition $\int |\Psi_i(\mathbf{R})|^2 d\mathbf{R} = N_i$. Here N_i , m_i and μ_i denote the number of atoms, mass of the atom, and the chemical potential of the i -th ($i=1$ & 2) component of BEC. κ is the quantum of circulation of atoms about the z axis. Ψ_1 and Ψ_2 are the center-of-mass (CM) wavefunctions of the components, say, BEC-1 and BEC-2. ω_\perp and ω_Z are trapping potentials in the $x-y$ plane and along the z axis, respectively. U_{11} and U_{22} are the intra-component coupling strengths of species 1 and 2, respectively. U_{12} and U_{21} are the inter-component coupling strengths between the species. These coupling strengths are related to intra- and inter-component s -wave scattering lengths via the relations, $U_{11} = 4\pi a_{11}\hbar^2/m_1$, $U_{12} = U_{21} = 2\pi a_{12}\hbar^2(m_1 + m_2)/m_1m_2$ and $U_{22} = 4\pi a_{22}\hbar^2/m_2$. Now atoms in each of the BEC components are considered to be of the simplest form, a valance electron of charge $-e$ and mass m_e roaming around core electron and nucleus of total charge $+e$ and mass m_n . The CM coordinate with respect to laboratory coordinate system is $\mathbf{R} = (m_e \mathbf{r}_e + m_n \mathbf{r}_n)/m_t$, where $m_t = m_e + m_n$ being the total mass. Here \mathbf{r}_e and \mathbf{r}_n are the coordinates of the valance electron and the center of atom, respectively, with respect to laboratory coordinate system and the relative (internal) coordinate can be expressed as $\mathbf{r} = \mathbf{r}_e - \mathbf{r}_n$.

We consider the LG beam without any off-axis node, propagating along the z axis of the laboratory frame. The beam interacts with the coupled BEC whose de Broglie wavelength is large enough to feel the intensity variation of the LG beam but smaller than the waist of the beam. Let ψ_i and Ψ_i be the internal (electronic) and the CM wavefunction, respectively, of i -th component of BEC. Then the total wavefunction of the system of two-component BEC can be written as, $\Upsilon(\mathbf{R}_1, \mathbf{R}_2, \mathbf{r}_1, \mathbf{r}_2) = \Psi_1(\mathbf{R}_1)\Psi_2(\mathbf{R}_2)\psi_1(\mathbf{r}_1)\psi_2(\mathbf{r}_2)$. Here the atom-radiation interaction Hamiltonian, H_{int} , is derived from the Power-Zienau-Wooley (PZW) scheme [65], which is beyond the level of dipole approximation.

$$H_{int} = - \int d\mathbf{r}' P(\mathbf{r}') \cdot \mathbf{E}(\mathbf{r}', t) + h.c. \quad (3)$$

where $\mathbf{E}(\mathbf{r}', t)$ is the local electric field of the LG beam [66, 67] experienced by the atom. $P(\mathbf{r}')$ is the electric polarization given by

$$P(\mathbf{r}') = -e \frac{m_n}{m_t} \mathbf{r} \int_0^1 d\lambda \delta\left(\mathbf{r}' - \mathbf{R} - \lambda \frac{m_n}{m_t} \mathbf{r}\right). \quad (4)$$

If the LG beam interacts with one of the components of the BEC (say, n -th), then the dipole transition matrix element under paraxial approximation will be

$$\begin{aligned}
 M_{i \rightarrow f}^n = \langle \Upsilon_f^i | H_{int} | \Upsilon_i \rangle &= \sqrt{\frac{4\pi}{3|l|!}} e \frac{m_n}{m_t} \sum_{\sigma=0,\pm 1} \epsilon_\sigma \\
 &\times \left[\langle \Psi_{nf}(\mathbf{R}_n) | \frac{R_n^{(|l|)}}{w_0^{|l|}} e^{il\Phi_n} e^{ikZ_n} | \Psi_{ni}(\mathbf{R}_n) \rangle \langle \psi_{nf}(\mathbf{r}_n) | r Y_1^\sigma(\hat{\mathbf{r}}) | \psi_{ni}(\mathbf{r}_n) \rangle \right. \\
 &\times \left. \prod_{p \neq n} \langle \Psi_{pf}(\mathbf{R}_p) | \Psi_{pi}(\mathbf{R}_p) \rangle \langle \psi_{pf}(\mathbf{r}_p) | \psi_{pi}(\mathbf{r}_p) \rangle \right], \quad (5)
 \end{aligned}$$

where $\epsilon_\pm = (E_x \pm iE_y)/\sqrt{2}$ and $\epsilon_0 = E_z$. Eq. (5) clearly shows that the azimuthal coordinate (Φ_n) of the CM is changed by nucleation of vortex dictated by the topological charge of the beam. The polarization of the field interacts with the electronic motion, resulting in an electronic transition between the two internal states of the atoms. This portion of the transition matrix element is calculated using relativistic coupled-cluster theory [68, 69, 70]. Since both the components of the BEC are coupled by an inter-component coupling, the creation of vortex in one of the components directly affects the wavefunction of another component of the BEC. But, here we consider changes that occur only on the CM wavefunction of the latter component for the sake of simplicity and the minor effect on their electronic motion is neglected.

In the next section, we study numerical results of two-photon stimulated Raman transition using co-propagating LG and Gaussian beams and discuss the variation of the Rabi frequencies under the variation of inter-component coupling strength.

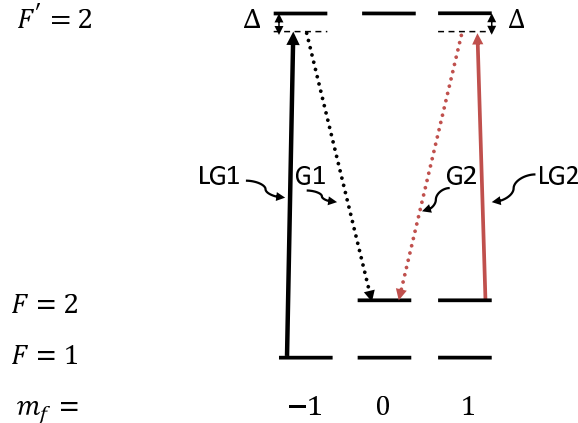


Figure 1. Energy level scheme of the two-photon Raman transitions. The atomic states show the ^{87}Rb hyperfine states. Atoms are initially trapped in $|5s_{1/2}, F=1, m_f=-1\rangle$ and $|5s_{1/2}, F=2, m_f=1\rangle$. Δ represents two-photon detuning.

3. NUMERICAL RESULTS AND INTERPRETATION

We consider that the LG beam interacts with a coupled ^{87}Rb BEC prepared in $\psi_1 = |5S_{1/2}, F=1, m_f=-1\rangle$ and $\psi_2 = |5S_{1/2}, F=2, m_f=1\rangle$ hyperfine states

in a harmonic potential as discussed in the experimental work [1]. For simplicity, we consider that both the hyperfine states have been populated by equal number of atoms. We choose the characteristics of the experimental trap as given in Ref [71] with asymmetry parameter $\lambda_{tr} = \omega_Z/\omega_{\perp} = 2$ and the axial frequency $\omega_Z/2\pi = 40$ Hz. The characteristic length is $a_{\perp} = 4.673 \mu\text{m}$. The intra-component s -wave scattering lengths are $a_{11} = 1.03 \times 5.5 \text{nm}$, $a_{22} = 0.97 \times 5.5 \text{nm}$ [1] and the inter-component s -wave scattering length is $a_{12} = a_{21} = g \times 5.5 \text{ nm}$, where g is a parameter which can be tuned [29, 72]. The intensity of the LG beam is $I = 10^2 \text{ W cm}^{-2}$ and its waist $w_0 = 10^{-4} \text{ m}$.

The interaction of the trapped atoms with the LG beam has an extra physical degree of freedom than interaction with a Gaussian beam. The former interaction is expected to extract an extra physical feature of the BEC, like the orientation of vortex in the matter system [50]. These features are dependent to a large extent on the interaction among the atoms.

Initially, we consider that both the components of the BEC are in non-vortex states. Let the co-propagating LG and Gaussian (G) beams with appropriate polarization interact simultaneously with BEC-1, using stimulated Raman transition to $|5s_{\frac{1}{2}}, F = 2, m_f = 0\rangle$. The frequency difference between the two kinds of pulses, $\delta\nu_r$ is set equal to the recoil energy. The two-photon transitions are taken via $|5p_{\frac{3}{2}}, F' = 2, m_f = -1\rangle$. Here G beam is detuned from the D2 line by $\Delta = -1.5 \text{ GHz}$ (≈ -150 linewidths, enough to resist the destructive incoherent heating of the condensate due to spontaneous decay of excited states). Since the LG and G beams are co-propagating, the net transfer of linear momentum to the atom is zero. A similar case can be considered where the LG and G beams interact with BEC-2 as shown in the Fig. 1. As the figure shows, both the cases of Raman transitions lead to the same final electronic state. Again, simultaneous application of the above two sets of LG and G beams to the corresponding components of BEC lead to interference pattern at the final state, $|5S_{\frac{1}{2}}, F = 2, m_f = 0\rangle$. We would like to study the variation in interference patterns of a vortex-antivortex pair with the inter-component interaction strength. To investigate the interference patterns, we need to know the initial density profile of both the components and their interaction with LG beam in terms of Rabi frequencies.

3.1. Density profile of the components of BEC

Densities of BEC-1 and BEC-2 in the trap depend on the kinetic energy of the particles, external trapping potential, intra- and inter BEC interactions. The positive inter-BEC interaction helps de-mixing of the BEC components, means the overlapping region will decrease with the increase in the g -value. Whereas, in general, positive intra-BEC mean-field interaction is proportional to the number density of the particles. This means that the span of each of the components [73] increases with the increase of the density of atoms in it and this leads to more overlap in density profile among the components. Therefore, the number density of particles and inter-component interaction are anti-correlated for the overlap of the density profile of the BEC components. Further, the

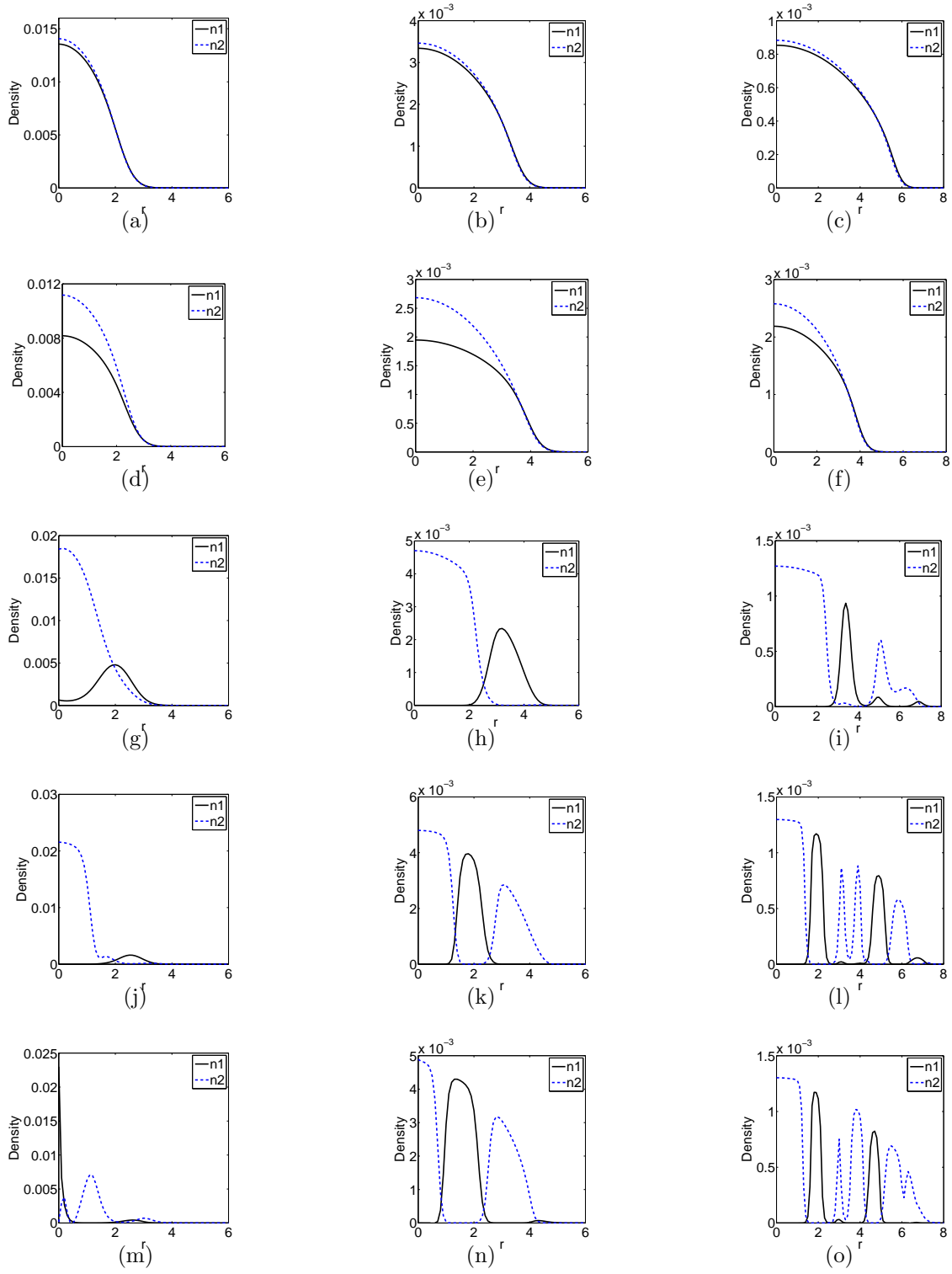


Figure 2. Plot of the density (in unit of a_{\perp}^{-3}) of BEC-1 (solid lines) and BEC-2 (dotted line) in the case of $N=10^5$ (1st column), $N=10^6$ (2nd column), and $N=10^7$ (3rd column). Rows correspond to $g = 0, 0.40, 0.70, 1.30$ and 1.60 . r is unit of a_{\perp} and both the states are non-vortex states.

trapping potential tries to confine the condensates and thus also defend the phase mixing among the components [55]. As a consequence, the initial density distributions of BEC-1 and BEC-2 over the extent of the trap are expected to be different for the different combination of the above parameters as discussed in the following paragraphs. As a result of simultaneous Raman transitions on the binary components, discussed in the last section, different structures of the interference patterns will emerge.

Let's start with non-vortex BEC components with different numbers of atoms and inter-component coupling as shown in Fig. 2 corresponding to $10^5, 10^6, 10^7$ numbers of atoms, each, for both the components of BEC. The plots presented here are at the level $z = 0$ of the trap having azimuthal symmetry.

Case-1: $g = 0$: (No coupling between BEC-1 and BEC-2) BEC-1 is more expanded than BEC-2 as former one has relatively large scattering length. Therefore, the central density of BEC-1 is always less compared to BEC-2 as shown in FIG. 2.

Case-2: $0.30 \leq g \leq 0.90$: (mutual interaction between the BEC components is essential) Here, many exciting features in density profiles are observed as the components start departing from each other. In all the cases, the central densities of both the components are reduced compared to the BEC states with $g=0$ as shown in the first row of Fig. 2. Now, when the inter-BEC interaction strength increases, BEC-1 continues its trend of decreasing density in the central region and eventually reaching the minimum. But BEC-2 is emerged with opposite trend, and its density is maximum at and near the center of the trap. The reason behind this is the competition between intra- and inter-component interactions. Signature of multi-ring shaped density profile is observed for $N = 10^7$.

Case-3: $g > 0.90$: (strong coupling between the components) As g increases further, the density of BEC-1 component is shifted away from the center of the trap. Whereas, BEC-2 gets concentrated near the center. With increasing population in the central region, BEC-2 breaks apart, and part of it grows at the outer surface of BEC-1 to form multi-ring shaped density profile in the x-y plane. Therefore, the fragmentation of the components is predicted for larger population as seen in last two rows of Fig. 2. g is considered here till 1.60 and beyond $g = 1.66$ the two-component system collapses for $N = 10^7$. This is the unusual situation which in general happens for the BEC with negative scattering length. The splitting can also happen for the smaller number of particles, but it needs a larger inter-component interaction (not shown in figures here). Here we do see that the fragments of different components repel each other more strongly as we increase the inter-component interaction strength. This may be the reason for the collapse. Also this critical value of g changes with the trap size which will be discussed later.

3.2. Interaction of BECs with LG beam

Now we would like to discuss the interaction of these two-component BECs with the LG beam having topological charge +1, say (physics will be similar for -1 also). FIG. 3

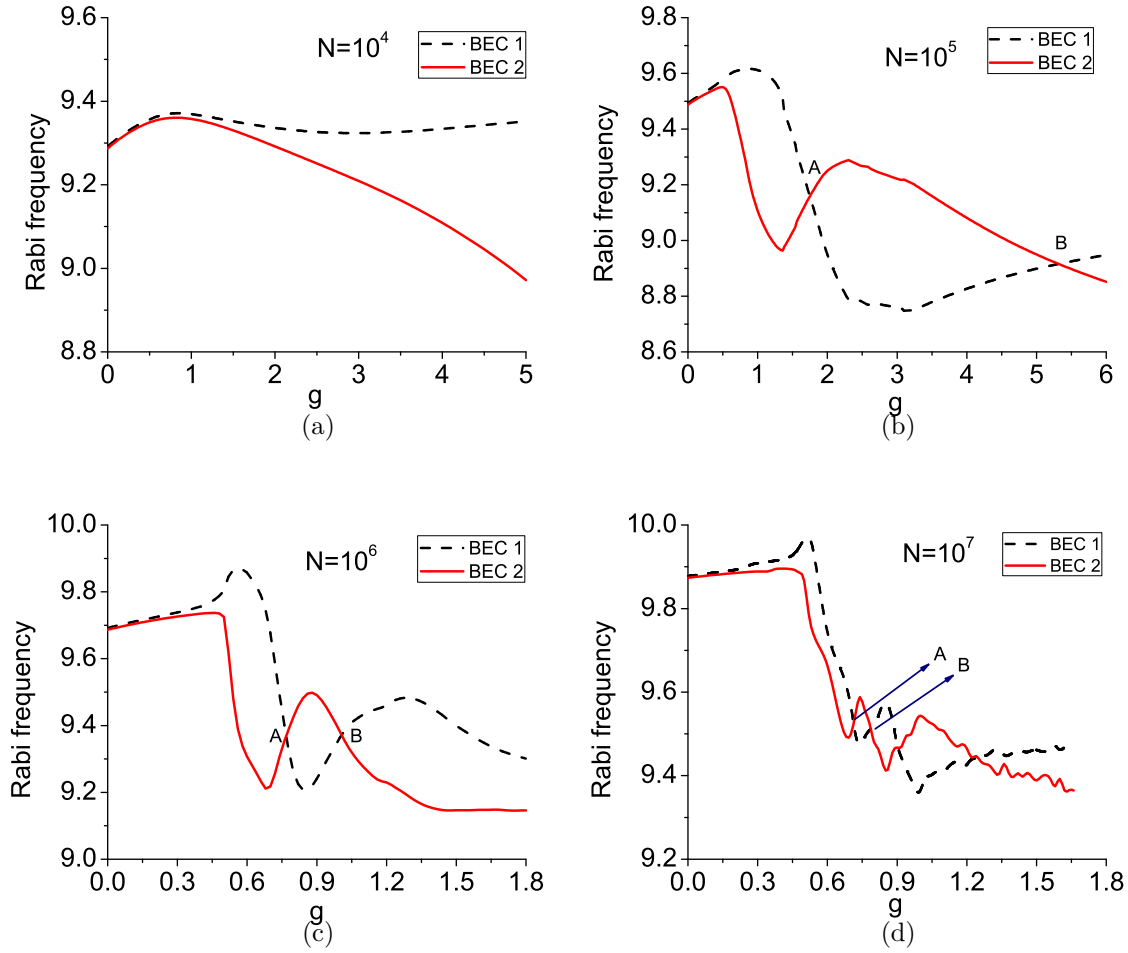


Figure 3. Variation of dipole Rabi frequency (in Sec^{-1}) of BEC-1 and BEC-2 with g on a semilog scale. LG beam of $\text{OAM}=+1$ interacts with non-vortex BECs.

presents the variation in Rabi frequencies of two-photon Raman transitions as described in FIG. 1, with respect to the g -value. All the density profiles used in the last section have been used here for initial wavefunctions of the components of BEC. Variations of the Rabi frequencies have been presented in the figure to show consistent behavior with other large populations at low g -values and to confirm no unusual feature for moderate or large g -values. The plot confirms that the BEC-2 component shrinks in the trap with the increasing inter-component interactions. For populations 10^5 or more, density profiles of BEC start showing unusual behaviour starting from $g = 0.5$. The components of BEC peak at different places, something like peaks of the BEC-1 and BEC-2 appear alternately. Therefore, the interaction of the BEC with the LG beam for these ranges of parameters is expected to provide interesting physics in terms of Rabi frequencies.

Having larger intra-component interaction, BEC-1 has relatively larger Rabi frequency than BEC-2 in the region of weak inter-component coupling (i.e. $g \leq 0.5$). This is due to the larger overlap of the beam profile with BEC-1 than BEC-2. Both the Rabi frequencies are increasing initially in this region of g because of the uniform

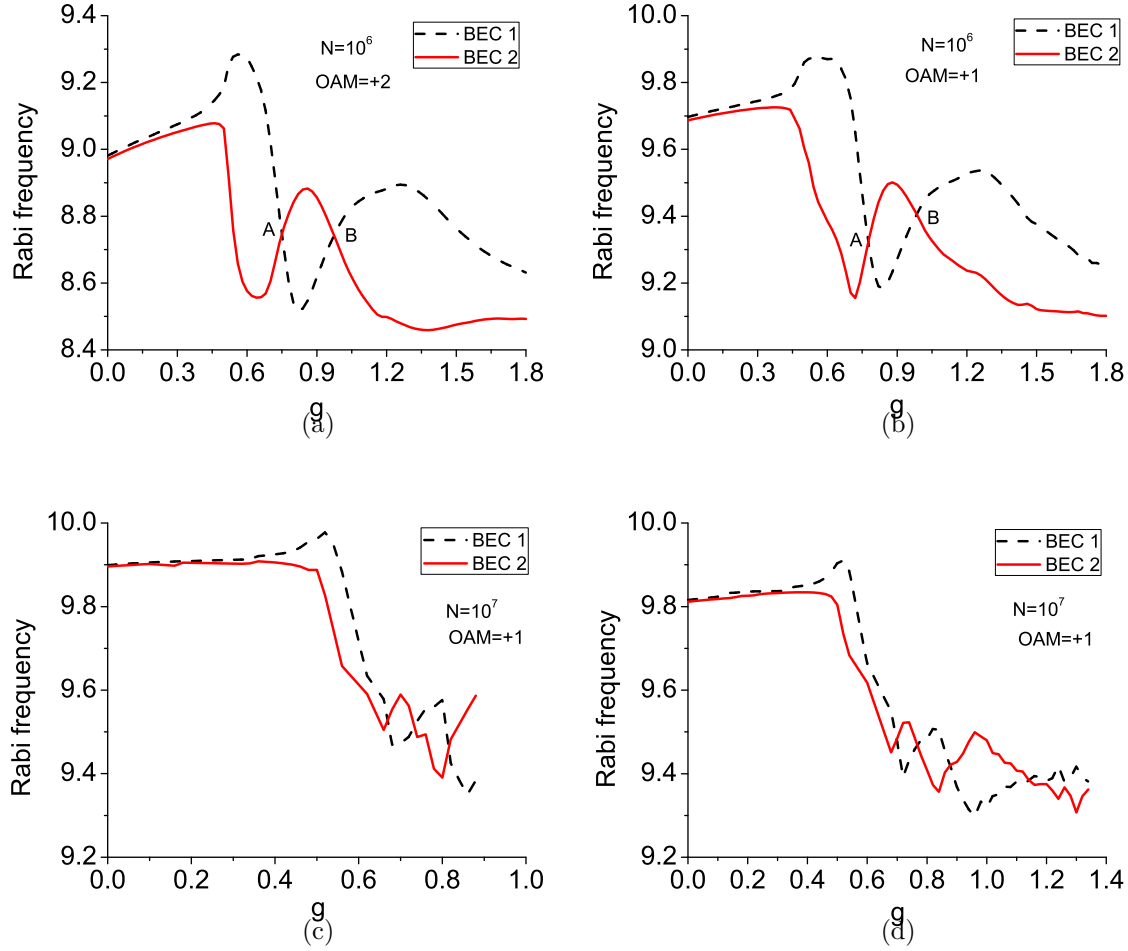


Figure 4. Variation of dipole Rabi frequency (in Sec^{-1}) of BEC-1 and BEC-2 with g on a semi-log scale. LG beam interacts with non-vortex BECs with $N = 10^6$ for (a) $a_{11} = 1.03 \times 5.5\text{nm}$, $a_{22} = 0.97 \times 5.5\text{nm}$ and (b) $a_{11} = 1.06 \times 5.5\text{nm}$, $a_{22} = 0.94 \times 5.5\text{nm}$. For $N = 10^7$ with $a_{11} = 1.03 \times 5.5\text{nm}$, $a_{22} = 0.97 \times 5.5\text{nm}$ and (c) $a_{\perp} = 3 \mu\text{m}$ and (d) $a_{\perp} = 4 \mu\text{m}$.

enlargement of the span of matter density and it accelerates with the population of atoms.

The initial reduction of Rabi frequencies of BEC-2 is consistent with the fast collapse of its density over radial span with increasing g -values. Further, the density collapse is estimated faster with respect to g -values as total population in the system increases. The trend is similar for BEC-1, though its collapse occurs at relatively larger values of g as its density profile has stronger overlap with beam profile up to the relatively larger values of g . Interestingly, the separation between the collapse regions of g -values for both the components is narrowing down with the increase in total populations and almost overlap around 0.5 to 0.7 for $N = 10^7$.

This can be understood if we compare the density profiles of the components around the radial region of two times the characteristic length of the trap, where the intensity

profile of the LG beam is also significant.

One of the striking features of the distribution of Rabi frequencies displayed in FIG. 3, is that the hierarchy of strength of Rabi frequencies between BEC-1 and BEC-2 is exchanged at certain values of g . These degenerate points in the plots are denoted as 'A' and 'B'. The separation of A and B points is reduced with the increase of the number of particles. In FIG 3 (d), the hierarchy between the Rabi frequencies gets phase changed multiple times within $g = 2$. Here the arbitrariness of the lengths between 'A' and 'B'-type critical points is because of the instabilities of the BECs at higher g -values.

To understand the dependency of the distribution on different parameters of the beam, trap geometry and properties of atoms, we consider the cases where a particular parameter is changed keeping all the other parameters fixed as discussed for FIG. 3. FIG. 4 displays the variation of Rabi frequencies over the range of g . FIG. 4(a) shows variation of Rabi frequencies for $N = 10^6$, OAM=+2. It is clear that the crossing points, A and B, of the distribution, have a negligible dependence on the charge of the optical vortex when it is compared with FIG 3(c). But the maximum difference between the distributions in between the points A and B has increased in the latter case, and this can reduce the visibility of the interference pattern discussed in the next section. FIG. 4(b) displays the same variation as FIG 3(c), but $(a_{11}, a_{22}) = (1.06, 0.94) \times 5.5nm$. Here we see significant effect compared to FIG 3(c) where $(a_{11}, a_{22}) = (1.03, 0.97) \times 5.5nm$ is used. FIG. 4(c) and FIG. 4(d) show the fluctuations of Rabi frequencies for tighter trapping potentials with $a_{\perp} = 3\mu m$ and $a_{\perp} = 4\mu m$, respectively, in case of $N = 10^7$. We observe multiple crossings between the spectrum of Rabi frequencies for BEC-1 and BEC-2. As expected, the components of BEC are collapsed at lower g -values: 0.88 and 1.34, respectively.

4. CREATION OF VORTEX-ANTIVORTEX STATES WITH EQUAL AND UNEQUAL QUANTUM CIRCULATION

Formation of the quantized vortex and antivortex, and their superposition in the BEC by the LG beam have been experimentally studied [71, 74] over last decade to understand the properties of vortices in BEC. The coherent superpositions of vortex-antivortex of equal or unequal circulation quantum numbers [74, 75] yield interesting interference effects with potential applications [76, 77], such as manipulating the chirality [50, 51, 78]. In these studies, the matter-wave vortex is shown to acquire vorticity equal to the winding number of the LG beam corresponding to electronic dipole transition.

To make this superposition, let us consider that the LG beam with positive vorticity interacts with BEC-1 and negative vorticity with BEC-2 as shown in FIG.1. The two-photon Raman transitions produce vortex-antivortex pair in the hyperfine state $|\psi_i\rangle = |5S_{\frac{1}{2}}, F = 2, m_f = 0\rangle$. The interference pattern of the superposition will depend on the populations of the vortex states. Thus the Rabi frequencies corresponding to these two-photon transitions are important for the coherency of the interference pattern.

In general, the two different macroscopic vortices with vorticities l_1, l_2 superpose

with arbitrary proportion as [51, 53]

$$\Psi(R, \Phi, Z, t) = f(R, Z)e^{-i\mu t}(\alpha_1 e^{il_1\Phi} + \alpha_2 e^{il_2\Phi}), \quad (6)$$

where $R^2 = (X^2 + Y^2)$, μ is chemical potential of the system. The constants, α_1 and α_2 , depend on the strengths of two-photon transitions corresponding to vortex and antivortex, respectively, with $|\alpha_1|^2 + |\alpha_2|^2 = 1$. All the density structures presented in Fig. 5 are at $Z = 0$ plane. The left and right columns of FIG. 5 present the density profile of $N = 10^6$ BEC at vortex-antivortex superposed state for $g = 0.76$ and $g = 0.86$, respectively. Here, choice of quantum circulation are $(l_1, l_2) = (1, -1)$ for 5(a) and 5(b), $(l_1, l_2) = (1, -2)$ or $(2, -1)$ for 5(c) and 5(d), and $(l_1, l_2) = (2, -2)$ for 5(e) and 5(f). The choice of $g = 0.76$ is considered here for $|l_1| = |l_2|$ to show the coherent interference where the populations of both the components are equal. We get same interference pattern also at the point 'B' as well as at $g = 0$ where there is no interaction among the components. In the same spirit, $g = 0.86$ (between A and B points) is chosen where maximum deviation of Rabi frequencies occurs. First and third rows of FIG. 5 show symmetric fringe patterns with respect to X and Y axes due to equal amplitudes of l_1 and l_2 . Whereas, second row is one of the examples of superposition of vortex and antivortex with unequal quantum circulation number. Also, the observation of distributions of Rabi frequencies for BEC-1 and BEC-2 (FIG. 3(c) and FIG. 4(a)) justify why the visibility in this case is much better for $g = 0.86$ than $g = 0.76$ for unequal quantum circulation number of vortex-antivortex. In all these interpretations, we keep in mind that approximately equal number of particles with opposite orientation can produce clear fringe pattern. In case of non-equal initial populations among BEC-1 and BEC-2, we will get similar patterns of interference at different values of g .

5. CONCLUSION

We have developed a theory of interaction of LG beam with binary mixtures of BEC and have shown the variability of the vortex-antivortex superposed state. Competition between intra- and inter-BEC interactions for the two-component non-vortex ground state has been shown in the graphical representation. The effects of the number of particles in this binary condensation have also been investigated. For $N = 10^7$, the critical value of g has been found out, for which the BECs collapse. The effects of the trapping potential on the critical values of g have also been studied along with the degeneracy points of Rabi frequencies. We have shown, how the wavefunctions of the initial states of the components directly affect the Rabi frequency of the two-photon stimulated Raman transition. Here the two photons of Raman transition are made of LG and G beam. The calculated Rabi frequencies help us to find out the population density of the vortices of each of the components. These changes in population density of vortex-antivortex states show the variation of interference patterns.

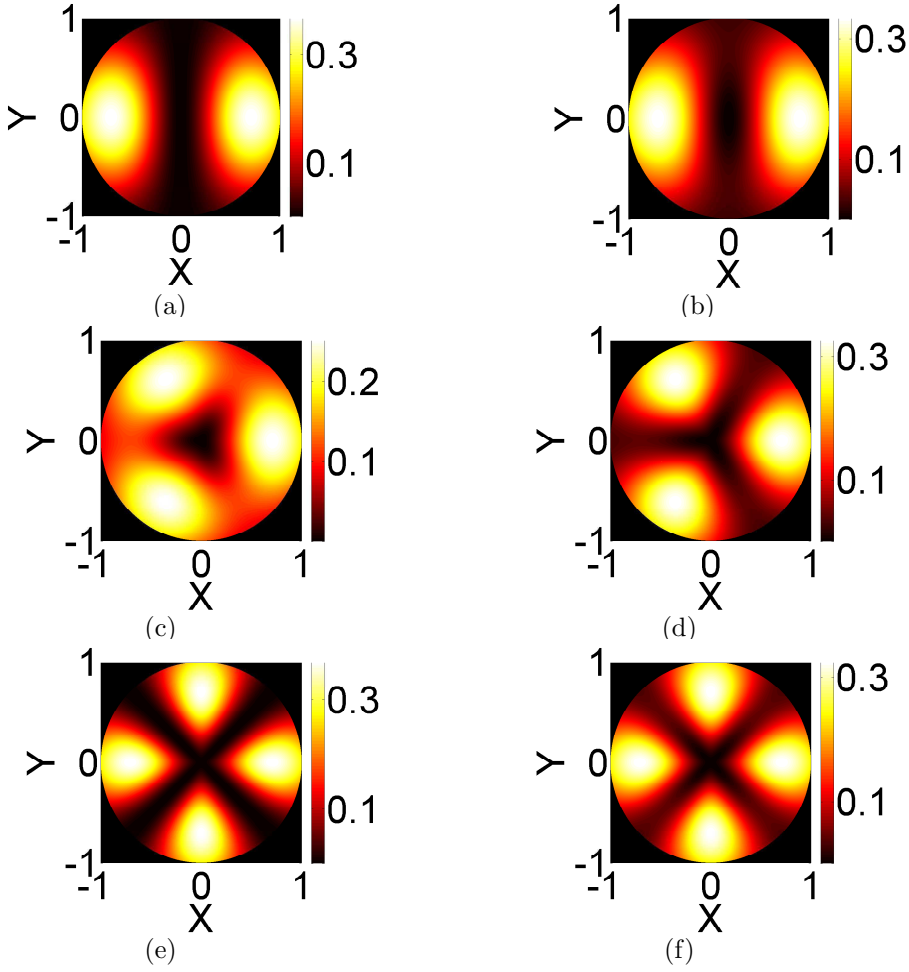


Figure 5. Plot of the density distribution of vortex-antivortex states of $N = 10^6$ with $(l_1, l_2) =$ (a)& (b)(1, -1), (c) & (d) (1, -2), (e) & (f) (2, -2). Left and right columns are for $g = 0.76$ and $g = 0.86$ respectively. All quantities are in dimensionless units.

ACKNOWLEDGMENTS

The calculations were performed in the IBM cluster at IIT-Kharagpur, India funded by DST-FIST.

APPENDIX

To derive the coupled-GP equations, we start from the action functional [64]

$$S = \int (\mathcal{L}_1 + \mathcal{L}_2 - U_{12}|\Psi_1|^2|\Psi_2|^2) d^3\mathbf{r} dt, \quad (7)$$

where the Lagrangian density of each component is

$$\mathcal{L}_k = i\frac{\hbar}{2} \left(\Psi_k^* \frac{\partial}{\partial t} \Psi_k - \Psi_k \frac{\partial}{\partial t} \Psi_k^* \right) - \frac{\hbar^2}{2m_k} |\nabla \Psi_k|^2 - V_k |\Psi_k|^2 - \frac{\kappa^2}{R^2} |\Psi_k|^2 - \frac{U_{kk}}{2} |\Psi_k|^4. \quad (8)$$

Here U_{kk} is the intra-atomic coupling strength and V_k is the external trapping potential.

Now, the coupled GP equations can be obtained by extremizing the action S with respect to Ψ_k^* using the equation $\frac{\partial S}{\partial \Psi_k^*} = 0$ [64]. Since the trapping potential $V_k = \frac{1}{2}m_k(\omega_\perp^2 R^2 + \omega_Z^2 Z^2)$, then the two-component GP equations take the form as

$$\left[-\frac{\hbar^2 \nabla^2}{2m_1} + \frac{1}{2}m_1(\omega_\perp^2 R^2 + \omega_Z^2 Z^2) + \frac{\kappa^2}{R^2} + U_{11}|\Psi_1|^2 + U_{12}|\Psi_2|^2 \right] \Psi_1 = \mu_1 \Psi_1, \quad (9)$$

$$\left[-\frac{\hbar^2 \nabla^2}{2m_2} + \frac{1}{2}m_2(\omega_\perp^2 R^2 + \omega_Z^2 Z^2) + \frac{\kappa^2}{R^2} + U_{22}|\Psi_2|^2 + U_{21}|\Psi_1|^2 \right] \Psi_2 = \mu_2 \Psi_2. \quad (10)$$

- [1] Hall D S, Matthews M R, Wieman C E, and Cornell E A 1998 Phys. Rev. Lett. **81** 1543
- [2] Myatt C J, Burt E A, Ghrist R W, Cornell E A, and Wieman C E 1997 Phys. Rev. Lett. **78** 586
- [3] Stamper-Kurn D M, Andrews M R, Chikkatur A P, Inouye S, Miesner H -J, Stenger J, and Ketterle W 1998 Phys. Rev. Lett. **80** 2027
- [4] Maddaloni P, Modugno M, Fort C, Minardi F, and Inguscio M 2000 Phys. Rev. Lett. **85** 2413
- [5] Matthews M R, Anderson B P, Haljan P C, Wieman C E, and Cornell E A 1999 Phys. Rev. Lett. **83** 2498
- [6] Anderson B P, Haljan P C, Wieman C E, and Cornell E A 2000 Phys. Rev. Lett. **85** 2857
- [7] Ho T -L and Shenoy V B 1996 Phys. Rev. Lett. **77** 3276
- [8] Jezek D M, Capuzzi P, and Cataldo H M 2001 Phys. Rev. A **64** 023605
- [9] Jezek D M, and Capuzzi P 2005 J. Phys. B: At. Mol. Opt. Phys. **38** 4389
- [10] Chui S T, Ryzhov V N, and Tareyeva E E 2000 J. Exp. Theor. Phys. **91** 1183
- [11] Chui S T, Ryzhov V N, and Tareyeva E E 2001 Phys. Rev. A **63** 023605
- [12] Chui S T, Ryzhov V N, and Tareyeva E E 2002 J. Exp. Theor. Phys. **75** 279
- [13] Law C K, Pu H, Bigelow N P, and Eberly J H 1997 Phys. Rev. Lett. **79** 3105
- [14] Ao P and Chui S T 1998 Phys. Rev. A **58** 4836
- [15] Timmermans E 1998 Phys. Rev. Lett. **81** 5718
- [16] Martin J L, McKenzie C R, Thomas N R, Sharpe J C, Warrington D M, Manson P J, Sandle W J, and Wilson A C 1999 J. Phys. B **32** 3065
- [17] Trippenbach M, Góral K, Rzazewski K, Malomed B, and Y.B. Band Y B 2000 J. Phys. B **33** 4017
- [18] Modugno G, Modugno M, Riboli F, Roati G, and Inguscio M 2002 Phys. Rev. Lett. **89** 190404
- [19] Thalhammer G, Barontini G, De Sarlo L, Catani J, Minardi F, and Inguscio M 2008 Phys. Rev. Lett. **100** 210402
- [20] McCarron D J, Cho H W, Jenkin D L, Köppinger M P, and Cornish S L 2011 Phys. Rev. A **84** 011603
- [21] Wacker L, Jørgensen N B, Birkmose D, Horchani R, Ertmer W, Klempt C, Winter N, Sherson J, and Arlt J J 2015 Phys. Rev. A **92** 053602
- [22] Wang F, Li X, Xiong D, and Wang D 2016 J. Phys. B **49** 015302
- [23] Lercher A D, Takekoshi T, Debatin M, Schuster B, Rameshan R, Ferlaino F, Grimm R, and Nägerl H -C 2011 Eur. Phys. J. D **65** 3
- [24] Pasquiou B, Bayerle A, Tzanova S M, Stellmer S, Szczepkowski J, Parigger M, Grimm R, and Schreck F 2013 Phys. Rev. A **88** 023601
- [25] Roy A and Angom D 2015 Phys. Rev. A **92** 011601(R)
- [26] Lee K L, Jørgensen N B, Liu I K, Wacker L, Arlt J J, and Proukakis N P 2016 Phys. Rev. A **94** 013602
- [27] Papp S B, Pino J M, and Wieman C E 2008 Phys. Rev. Lett. **101** 040402
- [28] Sugawa S, Yamazaki R, Taie S, and Takahashi Y 2011 Phys. Rev. A **84** 011610
- [29] Inouye S, Andrews M R, Stenger J, Miesner H -J, Stamper-Kurn D M, and Ketterle W 1998 Nature (London) **392** 151
- [30] Tojo S, Taguchi Y, Masuyama Y, Hayashi T, Saito H, and Hirano T 2010 Phys. Rev. A **82** 033609
- [31] Stenger J, Inouye S, Stamper-Kurn D M, Miesner H -J, Chikkatur A P, and Ketterle W 1998 Nature (London) **396** 345
- [32] Sadler L E, Higbie J M, Leslie S R, Vengalattore M, and Stamper-Kurn D M 2006 Nature (London) **443** 312
- [33] Sabbatini J, Zurek W H, and Davis M J 2011 Phys. Rev. Lett. **107** 230402
- [34] Hoefer M A, Chang J J, Hamner C, and Engels P 2011 Phys. Rev. A **84** 041605
- [35] Hamner C, Chang J J, Engels P, and Hoefer M A 2011 Phys. Rev. Lett. **106** 065302
- [36] De S, Campbell D L, Price R M, Putra A, Anderson B M, and Spielman I B 2014 Phys. Rev. A **89** 033631
- [37] Lee C 2009 Phys. Rev. Lett. **102** 070401
- [38] Kawakami T, Mizushima T, Nitta M, and Machida K 2012 Phys. Rev. Lett. **109** 015301

- [39] Ferrier-Barbut I, Delehaye M, Laurent S, Grier A T, Pierce M, Rem B S, Chevy F, and Salomon C 2014 Science **345** 1035
- [40] Mertes K M, Merrill J W, Carretero-González R, Frantzeskakis D J, Kevrekidis P G, and Hall D S 2007 Phys. Rev. Lett. **99** 190402
- [41] Eto Y, Takahashi M, Nabeta K, Okada R, Kunimi M, Saito H, and Hirano T 2016 Phys. Rev. A **93** 033615
- [42] Takeuchi H, Ishino S, and Tsubota M 2010 Phys. Rev. Lett. **105** 205301
- [43] Law K J H, Kevrekidis P G, and Tuckerman L S 2010 Phys. Rev. Lett. **105** 160405
- [44] Takeuchi H, Suzuki N, Kasamatsu K, Saito H, and Tsubota M 2010 Phys. Rev. B **81** 094517
- [45] Sasaki K, Suzuki N, Akamatsu D, and Saito H 2009 Phys. Rev. A **80** 063611
- [46] Ilo-Okeke E O and Byrnes T 2014 Phys. Rev. Lett. **112** 233602
- [47] Ilo-Okeke E O and Byrnes T 2016 Phys. Rev. A **94** 013617
- [48] Marzlin K -P, Zhang W, and Wright E M 1997 Phys. Rev. Lett. **79** 4728
- [49] Nandi G, Walser R, and Schleich W P 2004 Phys. Rev. A **69** 063606
- [50] Mondal P K, Deb B, and Majumder S 2015 Phys. Rev. A **92** 043603
- [51] Bhowmik A, Mondal P K, Majumder S, and Deb B 2016 Phys. Rev. A **93** 063852
- [52] Dutton Z and Ruostekoski J 2004 Phys. Rev. Lett. **93** 193602
- [53] Liu M, Wen L H, Xiong H W, and Zhan M S 2006 Phys. Rev. A **73** 063620
- [54] Simula T P, Nygaard N, Hu S X, Collins L A, Schneider B I, and Molmer K 2008 Phys. Rev. A **77** 015401
- [55] Wen L, Qiao Y, Xu Y, and Mao L 2013 Phys. Rev. A **87** 033604
- [56] Kapale K T and Dowling J P 2005 Phys. Rev. Lett. **95** 173601
- [57] Thanvanthri S, Kapale K T, and Dowling J P 2008 Phys. Rev. A **77** 053825
- [58] Wen L, Zhang Y, and Feng J 2010 J. Phys. B: At. Mol. Opt. Phys. **43** 225302
- [59] Nakamura Y, Pashkin Y A, and Tsai J S 1999 Nature London **398** 786
- [60] Friedman J R *et al.* 2000 Nature London **406** 43
- [61] van der Wal C H *et al.* 2000 Science **290** 773
- [62] Spedalieri F M 2006 Optics Communications, **260** 340
- [63] Pu H and Bigelow N P 1997 Phys. Rev. Lett. **80** 1130
- [64] G. P. Kevrekidis, D. J. Frantzeskakis, and R. Carretero-Gonzalez, eds., *Emergent Nonlinear Phenomena in Bose-Einstein Condensates* (Springer, Berlin, 2008).
- [65] Babiker M, Bennett C R, Andrews D L, and Dávila Romero L C 2002 Phys. Rev. Lett. **89** 143601
- [66] Mondal P K, Deb B, Majumder S 2014 Phys. Rev. A **89** 063418
- [67] Mukherjee K, Majumder S, Mondal P K, and Deb B 2018 J. Phys. B: At. Mol. Opt. Phys. **51** 015004
- [68] Bhowmik A, Dutta N N, and Roy S 2017 Astrophys. Journal **836** 125
- [69] Bhowmik A, Roy S, Dutta N N, and Majumder S 2017 J. Phys. B: At. Mol. Opt. Phys. **50** 125005
- [70] Das A, Bhowmik A, Dutta N N, and Majumder S 2018 J. Phys. B: At. Mol. Opt. Phys. **51** 025001
- [71] Andersen M F, Ryu C, Cladé P, Natarajan V, Vaziri A, Helmerson K, and Phillips W D 2006 Phys. Rev. Lett. **97** 170406
- [72] Chin C, Grimm R, Julienne P, and Tiesinga E 2010 Rev. Mod. Phys. **82** 1225
- [73] Dalfó F and Stringari S 1996 Phys. Rev. A, **53** 2477
- [74] Wright K C, Leslie L S, and Bigelow N P 2008 Phys. Rev. A **77** 041601(R)
- [75] Wright K C, Leslie L S, Hansen A, and Bigelow N P 2009 Phys. Rev. Lett. **102** 030405
- [76] Brachmann J F S, Bakr W S, Gillen J, Peng A, and Greiner M 2011 Opt. Express **19** 12984
- [77] Quinteiro G F and Kuhn T 2014 Phys. Rev. B **90** 115401
- [78] Toyoda K, Miyamoto K, Aoki N, Morita R, and Omatsu T 2012 Nano Letters **12**(7) 3645.